ISSN 1674-1056
http://cpb.iphy.ac.cn
http://iopscience.iop.org/cpb
中国物理 B
Chinese Physics
中国物理 Chinese Physics B

Electronic and magnetic properties of CrI_3 nanoribbons and nanotubes

Ji-Zhang Wang(王吉章), Jian-Qi Huang(黄建啟), Ya-Ning Wang(王雅宁), Teng Yang(杨腾), Zhi-Dong Zhang(张志东)

Citation: Chin. Phys. B . 2019, 28(7): 077301. **doi:** 10.1088/1674-1056/28/7/077301
Journal homepage: http://cpb.iphy.ac.cn; http://iopscience.iop.org/cpb

What follows is a list of articles you may be interested in

Tunable edge bands and optical properties in black phosphorus nanoribbons under electric field

Hong Liu(刘红)
Chin. Phys. B . 2018, 27(12): 127301. **doi:** 10.1088/1674-1056/27/12/127301

Distinct edge states and optical conductivities in the zigzag and armchair silicene nanoribbons under exchange and electric fields

Jianfei Zou(邹剑飞), Jing Kang(康静)
Chin. Phys. B . 2018, 27(3): 037301. **doi:** 10.1088/1674-1056/27/3/037301

Electronic states and spin-filter effect in three-dimensional topological insulator Bi_2Se_3 nanoribbons

Genhua Liu(刘根华), Pingguo Xiao(肖平国), Piaorong Xu(徐飘荣), Huiying Zhou(周慧英), Guanghui Zhou(周光辉)
Chin. Phys. B . 2018, 27(1): 017304. **doi:** 10.1088/1674-1056/27/1/017304

One-dimensional method of investigating the localized states in armchair graphene-like nanoribbons with defects

Yang Xie(谢阳), Zhi-Jian Hu(胡智健), Wen-Hao Ding(丁文浩), Xiao-Long Lü(吕小龙), Hang Xie(谢航)
Chin. Phys. B . 2017, 26(12): 127310. **doi:** 10.1088/1674-1056/26/12/127310

Band structure and edge states of star-like zigzag graphene nanoribbons

Hong Liu(刘红)
Chin. Phys. B . 2017, 26(11): 117301. **doi:** 10.1088/1674-1056/26/11/117301

Electronic and magnetic properties of CrI_3 nanoribbons and nanotubes*

Ji-Zhang Wang(王吉章)[1,2], Jian-Qi Huang(黄建啟)[1,2], Ya-Ning Wang(王雅宁)[1,2], Teng Yang(杨腾)[1,†], and Zhi-Dong Zhang(张志东)[1]

[1] *Shenyang National Laboratory for Materials Science, Institute of Metal Research, Chinese Academy of Sciences, Shenyang* 110016, *China*
[2] *School of Materials Science and Engineering, University of Science and Technology of China, Shenyang* 110016, *China*

(Received 11 April 2019; revised manuscript received 10 May 2019; published online 31 May 2019)

CrI_3 in two-dimensional (2D) forms has been attracting much attention lately due to its novel magnetic properties at atomic large scale. The size and edge tuning of electronic and magnetic properties for 2D materials has been a promising way to broaden or even enhance their utility, as the case with nanoribbons/nanotubes in graphene, black phosphorus, and transition metal dichalcogenides. Here we studied the CrI_3 nanoribbon (NR) and nanotube (NT) systematically to seek the possible size and edge control of the electronic and magnetic properties. We find that ferromagnetic ordering is stable in all the NR and NT structures of interest. An enhancement of the Curie temperature T_C can be expected when the structure goes to NR or NT from its 2D counterpart. The energy difference between the FM and AFM states can be even improved by up to 3–4 times in a zigzag nanoribbon (ZZNR), largely because of the electronic instability arising from a large density of states of iodine-5p orbitals at E_F. In NT structures, shrinking the tube size harvests an enhancement of spin moment by up to 4%, due to the reduced crystal-field gap and the re-balance between the spin majority and minority populations.

Keywords: CrI_3, nanoribbon, nanotube, magnetism

PACS: 73.20.At, 61.46.–w, 73.22.–f **DOI:** 10.1088/1674-1056/28/7/077301

1. Introduction

Two-dimensional (2D) van der Waals crystals have attracted broad attention due to their novel properties and potential applications in the last two decades.[1] The excellent mechanical,[2] electronic,[1,3–5] optical,[6–8] and especially magnetic properties[9] due to the quantum confinement effect have been widely reported. Isotropic long-range ferromagnetic (FM) order at low dimension has been proved to be thermodynamically unstable in Heisenberg systems from the Mermin–Wagner theorem.[10] However, a number of magnetic 2D-layered structures, such as $FePS_3$,[11] $Cr_2Ge_2Te_6$,[12–14] and CrI_3,[15,16] have recently been demonstrated by experiments to be stable with finite ordering temperature, largely due to the magnetic anisotropy and/or the Ising systems.[17–19] Among them, CrI_3 exhibits in-plane FM ordering but interlayer antiferromagnetic ordering (AFM).[15] Interestingly, the layer-dependent magnetic order can be switched by an electrical gating, for example, from an interlayer AFM ordering to ferromagnetic state between the layers in bilayer CrI_3 by electron doping.[20,21] Circular polarized photoluminescence has also been reported in CrI_3 monolayer.[22] Those findings may promise CrI_3 for applications in spintronics and optoelectronics.

Transforming 2D atomic-thick crystals into one-dimensional structures strengthens the quantum size effect in some manner and supplies a new playground for tuning electronic properties.[23–25] Especially, ribbon width and edge configuration in ribbon structures, tube diameter and chirality in nanotubes,[26] decoration style and end-size in nanowires[23] play essential roles on determining the emergent electronic and magnetic properties, as is the case with graphene nanoribbons,[27,28] MoS_2 nanoribbons,[29] transition metal chalcogenides nanowires,[30–32] and phosphorene nanoribbons.[33] So it is intriguing to know how different the electronic properties one can achieve or whether it is possible to enhance the magnetic properties through edge structures when bringing CrI_3 down from the 2D form to its ribbon or tube counterparts. Reports have barely been found in literature on this topic except for a computation study on the edge-tunable band structure in zigzag CrI_3 nanoribbons by Jiang *et al.*[34] A more systematic and thorough exploration on the size effect on the electronic and magnetic properties of CrI_3 nanoribbons and nanotubes is yet to be made.

In this paper, we studied the edge configuration and size dependent electronic and magnetic properties of CrI_3 nanoribbons (NRs) and nanotubes (NTs) by using first-principles density functional calculations. Typical zigzag and armchair edge configurations were chosen for both ribbon and tube structures, with ribbon width ranging from 12 Å to 70 Å. Both zigzag (ZZNR) and armchair nanoribbons (ACNR) are reasonably endothermic with respect to their 2D counterparts, with ZZNR slightly more stable than ACNR. Encouragingly,

*Project supported by the National Key R&D Program of China (Grant No. 2017YFA0206301) and the Major Program of Aerospace Advanced Manufacturing Technology Research Foundation NSFC and CASC, China (Grant No. U1537204).

†Corresponding author. E-mail: yangteng@imr.ac.cn

© 2019 Chinese Physical Society and IOP Publishing Ltd

the Curie temperature for both nanoribbons and nanotubes (ACNT and ZZNT), as evaluated from the energy difference between the FM and AFM states, is obviously enhanced from the CrI_3 2D crystals. Part contribution is due to the increased spin moment, especially in the case of nanotubes in which the spin moment of Cr is increased by 4%. Iodine edge atoms are also found to contribute to the increased magnetization in the ribbons. Moreover, the band gap E_g of ZZNR increases with increasing ribbon width, while in contrast, the band gap of ACNR and nanotubes (ACNT, ZZNT) decreases with increasing ribbon width and tube diameter unexpectedly. More interestingly, oscillations of band gap size and spin moment of ACNT with ribbon width were found, which may be ascribed to the quantum confinement and the crucial effect of the edges.[27] Polarized optical absorption was also calculated and found to occur in the whole Brillouin zone, due to parallel flat valence and conduction bands, which is promising for optoelectronic applications.

2. Methods

We used *ab initio* density functional theory with the exchange–correlation functional of Perdew, Burke, and Ernzerhof (PBE) flavor[35] as implemented in the Vienna *ab initio* simulation package (VASP).[36] The cut-off energy for the plane-wave basis set was set to be 350 eV. The Monkhorst–Pack scheme[37] was used to sample the Brillouin zone (BZ) over a $16\times1\times1$ k-mesh. The energy difference threshold for electronic self-consistency was set to be 10^{-7} eV. We used the plus U method with $U=2.65$ eV for the Cr atom.[38] All the structures were fully relaxed with the method of conjugate gradients[39] until the atomic force was less than 0.02 eV/Å. The van der Waals interaction was taken into account for all the structures. The vacuum space between two neighboring slabs was set to be 15 Å to avoid the artificial inter-slab interactions.

To evaluate the optical absorption, the electron-photon matrix element $M(c,v,\boldsymbol{k})$ was computed based on the Fermi golden rule to obtain the absorption probability α,

$$\alpha(\boldsymbol{k},E_L) = \frac{2\pi}{\hbar}\sum_{c,v}|M(c,v,\boldsymbol{k})|^2\,\delta(\epsilon_c(\boldsymbol{k}) - \epsilon_v(\boldsymbol{k}) - E_L), \quad (1)$$

in which the electron-photon matrix element $M(c,v,\boldsymbol{k})$ is[40–42]

$$M(c,v,\boldsymbol{k}) = \frac{e\hbar^2}{mE_\gamma}\sqrt{\frac{I}{c\epsilon_0}}\,e^{i(\omega_f-\omega_i\pm E_\gamma/\hbar)t}\boldsymbol{D}(c,v,\boldsymbol{k})\cdot\boldsymbol{P}, \quad (2)$$

where m is the carrier mass, ϵ_0 is the dielectric constant of vacuum, I is the intensity of the incident laser, $\boldsymbol{D}(c,v,\boldsymbol{k})$ $(=\langle\psi^c(\boldsymbol{k})|\nabla|\psi^v(\boldsymbol{k})\rangle)$ is the dipole vector taking care of the photon-excited electronic transition from valence state $\psi^v(\boldsymbol{k})$ to conduction state $\psi^c(\boldsymbol{k})$, and $\boldsymbol{P}$ is the laser polarization. Jone vectors (1, ±i, 0) were used to simulate the circular polarization of laser.

3. Results and discussion

In the following, we shall discuss the size dependence of the electronic and magnetic properties of CrI_3 nanoribbons and nanotubes.

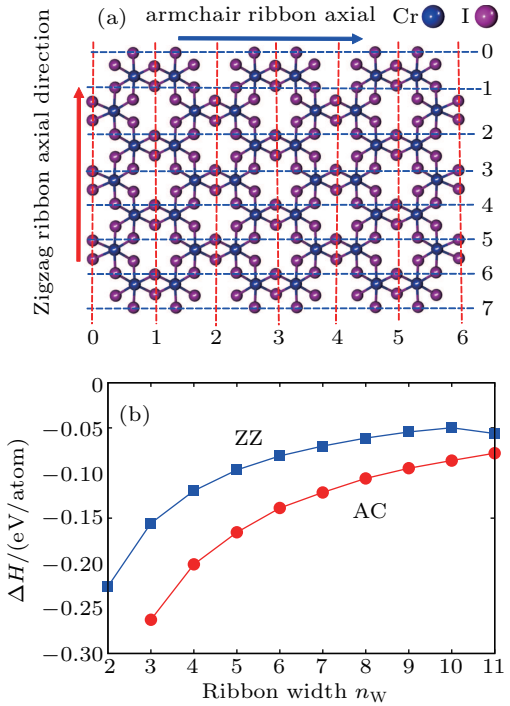


Fig. 1. (a) Definition of CrI_3 ribbon structures with zigzag and armchair edges. Arrows in red and blue show periodic axial directions of ZZ and AC ribbons, respectively. Dashed lines with numbers define the width index n_W. (b) The n_W dependence of formation enthalpy ΔH of both ZZNR and ACNR, ΔH is defined in Eqs. (3) and (4).

3.1. CrI_3 nanoribbons

Let us firstly define the ribbon structures for CrI_3. Two typical structures of ZZNR and ACNR are defined according to the sublattice of Cr atoms (blue), similar to the definition of graphene nanoribbon type, as shown in Fig. 1(a). Iodine atoms (purple) are selected to terminate the dangling bonds in Cr edge atoms for both types of ribbons, because it costs much more energy to have edge Cr atoms with dangling bonds from our formation enthalpy calculations. Guided by this rule, the edge structures with various ribbon widths were constructed, as highlighted in Fig. 1(a) by red and blue dashed lines and width index n_W for ZZNR and ACNR, respectively. To estimate the relative stability of ribbons with respect to the 2D CrI_3 crystal, the formation enthalpy ΔH for ZZNR and ACNR were calculated based on the following equations:

$$\frac{2+6n_W}{3}E_{CrI_3} = E_{ZZ} + \frac{2}{3}E_{Cr} + \Delta H, \quad (3)$$

$$\frac{4+6n_{\rm W}}{3}E_{\rm CrI_3} = E_{\rm AC} + \frac{4}{3}E_{\rm Cr} + \Delta H, \quad (4)$$

where $E_{\rm CrI_3}$, $E_{\rm Cr}$, $E_{\rm ZZ}$, and $E_{\rm AC}$ are respectively the total energies of 2D CrI_3, elementary Cr solid, ZZNR, and ACNR. Each ZZNR with width index $n_{\rm W}$ consists of $2n_{\rm W}$ Cr atoms and $2+6n_{\rm W}$ I atoms, while each ACNR has $2n_{\rm W}$ Cr atoms and $4+6n_{\rm W}$ I atoms.

As evident by the negative formation enthalpy given in Fig. 1(b), it is always endothermic to obtain ribbon structures of any type from 2D CrI_3. With decreasing ribbon width, ΔH normalized by the total number of atoms increases, suggesting that it is more difficult to get the narrower ribbon. ZZNR is more stable than ACNR at similar width, probably due to the energy gain from dimerization of the edge iodine pair in ZZNR compared with the single iodine edge atom in ACNR.

Firstly we studied the electronic properties of ZZNR, specifically the electronic band structure, magnetic properties, and relative stability between FM and AFM states, as shown in Fig. 2. The typical spin alignments of FM/AFM states are schematized in Fig 2(a), with the spin moment of Cr atoms pointing out of the structural basal plane from magnetocrystalline anisotropy calculation. The Curie temperature $T_{\rm C}$ can be estimated upon both the exchange stiffness J and saturated magnetization m according to the Weiss–Heisenberg model.[40] Exchange stiffness J can be calculated from energy difference $\Delta E_{\rm AFM-FM}$ between AFM and FM states.[43] In Figs. 2(b)–2(d), we show the ribbon-width-normalized $\Delta E_{\rm AFM-FM}$ and spin moment m as a function of $1/W$. As seen from Fig. 2(b), FM remains more stable than AFM regardless of the ribbon width (which is consistent with the results from Ref. [34]), and J can be increased by up to 3–4 times from 2D CrI_3 to ZZNR structures (width index $n_{\rm W} \geq 5$). Spin moment m in Fig. 2(c) does not show much improvement upon the 2D counterpart. But the spin charge density $\Delta\rho_{\rm FM}$ indicated in Fig. 2(d) shows some additional contribution from the edge iodine atoms in the ZZNR (left panel) compared to the 2D crystal (right panel). It is most likely to obtain an enhancement of $T_{\rm C}$ of the ribbon structures upon the bulk (61 K) and monolayer CrI_3 (45 K).[15,44]

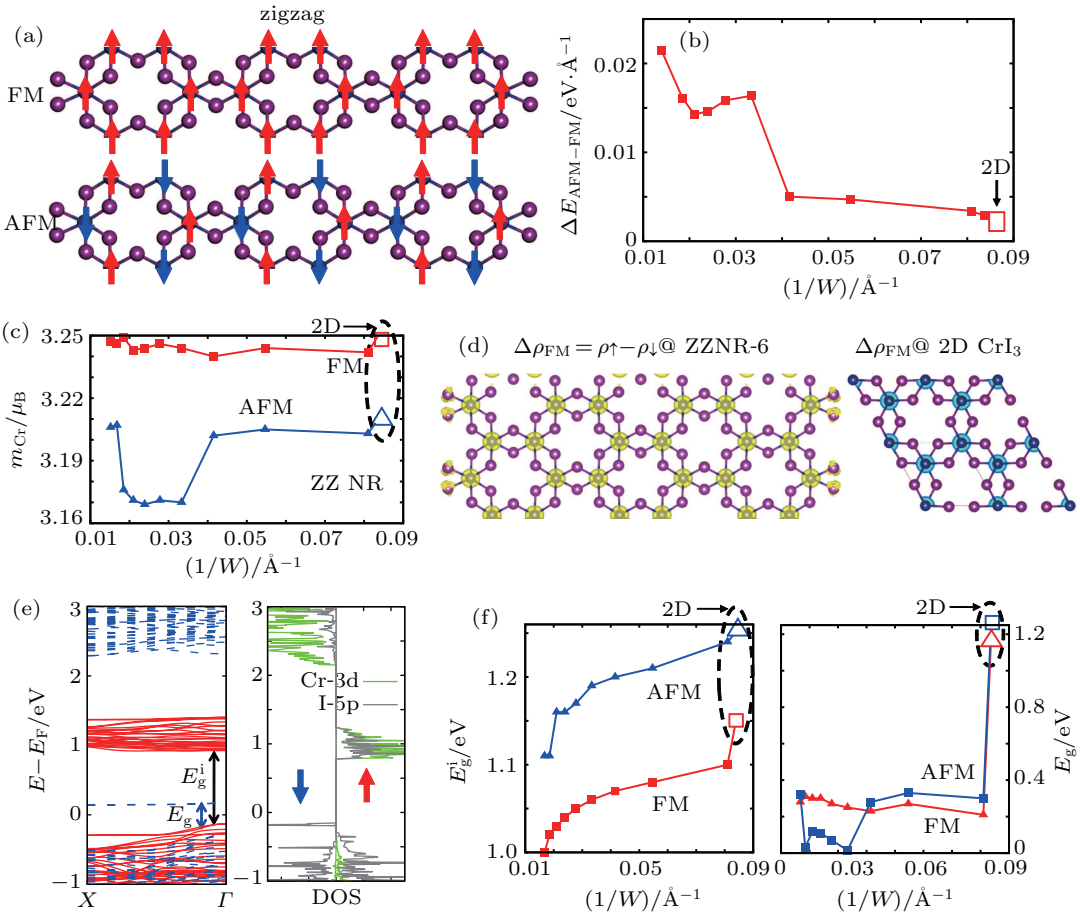


Fig. 2. (a) Schematic spin alignment on Cr atoms for both FM and AFM states in ZZNR. Up arrow (red) represents spin majority and down arrow (blue) spin minority. (b) Energy difference $\Delta E_{\rm AFM-FM}$ ($= E_{\rm AFM} - E_{\rm FM}$) for ZZNR as a function of inverse ribbon width. (c) Maximal magnetic moment for Cr atoms in FM (red square) and AFM (blue triangle) states in ZZNR as a function of $1/W$. (d) Spin charge density $\Delta\rho_{\rm FM}$ between spin majority and minority states for ZZNR-$n_{\rm W}$ ($n_{\rm W} = 6$) and 2D CrI_3 with $\Delta\rho = 0.118$ e/Bohr^{-3}. (e) Electronic band structure and projected density of states (PDOS) for ZZNR-6. The Cr-3d and I-5p orbitals are shown in green and gray lines, respectively. (f) Band gap of both FM and AFM states as a function of $1/W$. $E_{\rm g}^{\rm i}$ (left panel) and $E_{\rm g}$ (right panel), as defined in the band structure in (e), represent intrinsic and spin-flip band gaps, respectively.

To have more insight into the magnetic property, we calculated the electronic band structure and density of states (DOS), as showed in Fig. 2(e). The projected DOS on the right panel of Fig. 2(e) illustrates that not only the Cr-d orbitals (in green) but also the I-p orbitals (in grey) contribute to the net spin moment, especially the flat bands due to the I-5p orbitals near the Fermi level. The electronic instability arising from a large DOS of I-5p orbitals and the electron–electron Coulomb repulsion occurs at $E_{\rm F}$, which gives rise to a splitting of spin majority and minority bands. This is a new feature for the ribbon structures, which is not observed in the 2D counterpart. Band gap $E_{\rm g}$ due to the spin splitting, as defined in the band structure in Fig. 2(e), is about 0.2–0.3 eV (which is similar to the result in Ref. [34]), almost independent on the ribbon width, as seen from the right panel in Fig. 2(f). The optical absorption across $E_{\rm g}$ should be forbidden due to the electric-dipole selection rule ($\Delta l = \pm 1$, $\Delta m_{\rm s} = 0$), which is the case from the calculated optical absorption in Fig. 3. Meanwhile, the band gap $E_{\rm g}^{\rm i}$ of the spin majority bands between the I-5p and Cr-4d, as defined in Fig. 2(e), should be optically active due to $\Delta l = \pm 1$, as confirmed also in Fig. 3. In contrast to the spin flip band gap $E_{\rm g}$ independent of the ribbon width, $E_{\rm g}^{\rm i}$ increases with decreasing ribbon width W, obviously due to the quantum size effect.

Helicity dependence of photoluminescence was reported in 2D CrI_3 monolayer and bilayer.[22] It is worth checking whether it exists in the one-dimensional ribbon structure. We show the wave-vector, laser-energy, and (linearly and circularly) polarization dependence of optical absorption in Fig. 3. The optical gap of the spin majority band is smaller than the minority one. Due to many flat bands, the wave-vector independence of the optical absorption is obviously observed. It is

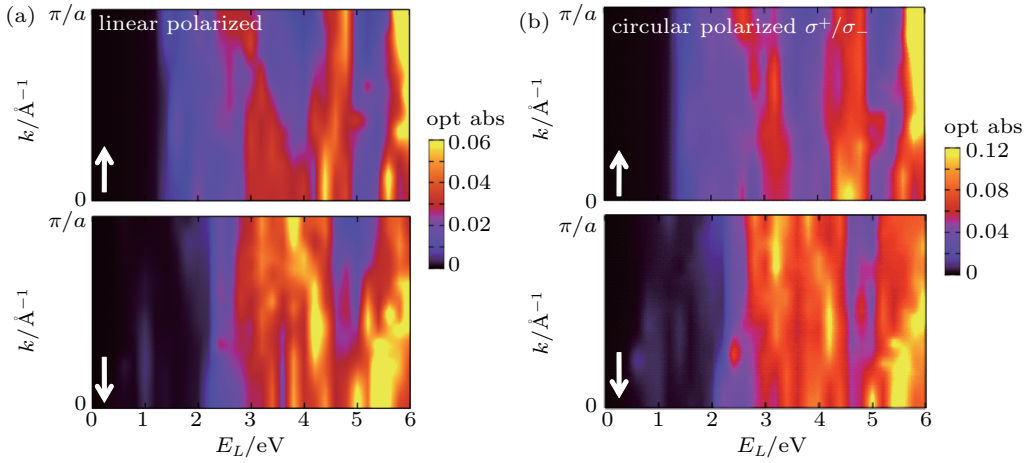


Fig. 3. The optical absorption of FM ZZNR-2 with spin and momentum resolution for (a) linear polarized laser and (b) circular polarized laser. Up and down arrows in the lower left corner show majority and minority spins, respectively.

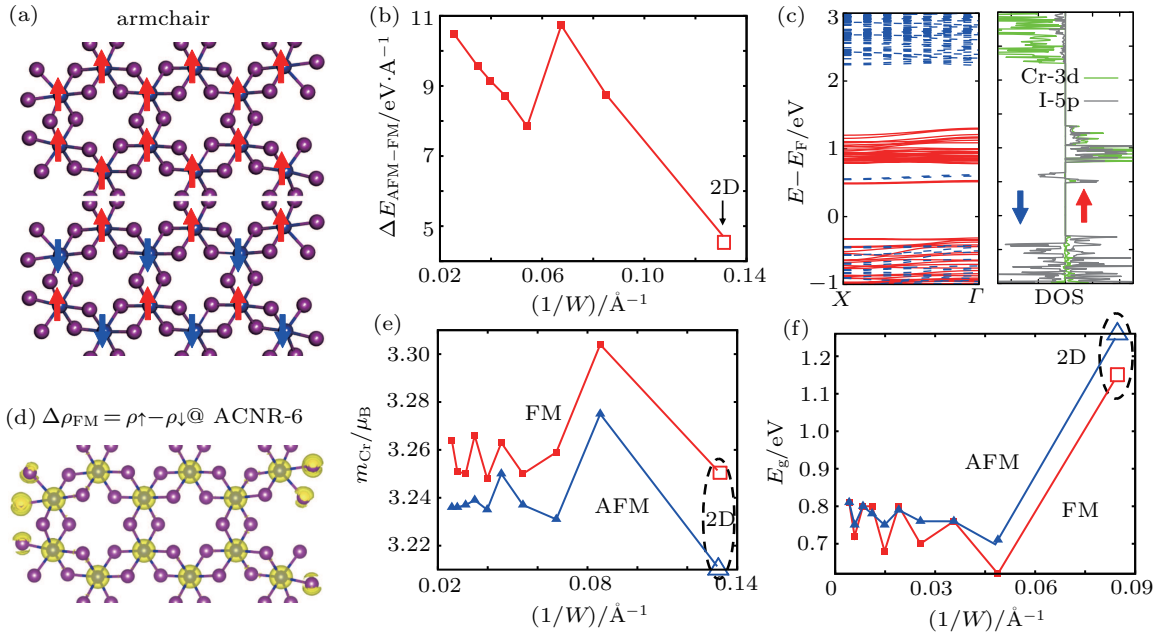


Fig. 4. Ribbon width dependence of electronic properties of ACNR. (a) FM and AFM spin alignments of Cr atoms. (b) Width normalized energy difference $\Delta E_{\rm AFM-FM}$ ($= E_{\rm AFM} - E_{\rm FM}$). (c) Band structure and projected DOS for ACNR-6. (d) Net spin charge density $\Delta\rho_{\rm FM}$. (e) Maximal magnetic moment of Cr atoms in both FM and AFM states. (f) Band gap $E_{\rm g}$ of both FM and AFM states.

a pity that no circular polarization dependence is found, namely, the helicity of both σ^+ and σ^+ gives the same result in Fig. 3(b). Circular polarized laser leads to two times as big intensity as the linear polarized laser, basically due to the fact that circular polarization is due to two linearly polarized lasers with 90° phase difference.

The edge type has been seen to significantly change the electronic and magnetic properties of NRs such as carbon NRs,[27] phosphorene NRs,[33] and MoS_2 NRs.[29] Besides the zigzag edge in honeycomb lattices, the armchair edge is another typical structure. Now let us shift from ZZNR to ACNR to see the edge structure effect on the electronic properties of nanoribbons. The spin configurations for both AFM and FM states are given in Fig. 4(a). It is encouraging to anticipate that the Curie temperature T_C will be much improved upon 2D CrI_3 as well in ACNR, largely thanks to the much enhanced exchange stiffness J as shown in Fig. 4(b) and slightly increased spin moment m as shown in Fig. 4(e). The discussion on ACNR will, therefore, be similar to that on ZZNR. However, the oscillation of both spin moment m_{Cr} and band gap E_g with the ribbon width W is unique in ACNR, as indicated in Figs. 4(e) and 4(f). Similar results have also been reported in graphene nanoribbons with armchair edge.[27] So likewise, we may ascribe such an oscillation of band gap E_g as well as of m with ribbon width in the ACNR to both quantum confinement and the crucial effect of the edges.[27]

3.2. CrI_3 nanotubes

Compared to ribbon structures with dangling bonds at the edge, tubular structures without edges should be more advantageous for many applications. But how about the magnetic properties in the tubular structures? Here we studied CrI_3 nanotubes with two typical chiralities, ZZNT(n, 0) and ACNT(n, n). Figure 5(a) shows the top view and side view of two representative nanotubes, ZZNT(6,0) and ACNT(6,6). Diameter D is defined as the largest distance between two furthest iodine atoms in the cutting plane perpendicular to the tube axial direction. The strain energy is evaluated in Fig. 5(b). In contrast to the weak dependence of strain energy on ribbon width in ZZNR and ACNR, the strain energy of NTs is inversely proportional to the square of the nanotube perimeter W (or diameter D), namely, $E/N_{Cr} \sim \alpha/D^2$, with $\alpha = 24.03$ eV·Å^2. The weak dependence of strain energy on tube chirality is very similar to that in carbon nanotubes and other tubular structures.[26] Our calculation results show that the FM state is energetic favorable compared to the NM and AFM states of CrI_3 NT, and the energy difference between the FM and AFM states is about 20 meV per Cr atom in CrI_3 NT.

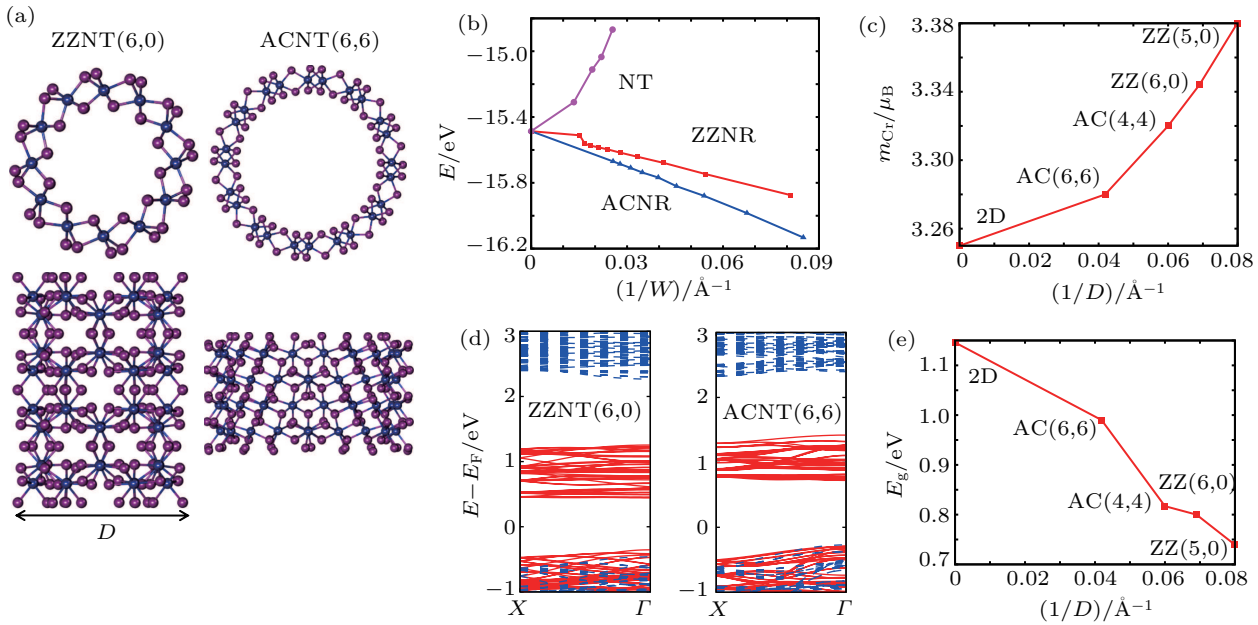


Fig. 5. Tube-size dependence of electronic properties of CrI_3 nanotubes. (a) Top view and side view of two chiralities (left: ZZNT(6,0) and right: ACNT(6,6)). (b) The $1/W$ dependence of total energy normalized by the number of Cr atoms for both nanotubes and nanoribbons. For NT, W is defined as the perimeter of the tube $W = \pi D$, with D being the diameter. (c) Maximal magnetic moment of Cr atom as a function of inverse diameter $1/D$. 2D CrI_3 sheet is also shown at $1/D = 0$. (d) Band structures for ZZNT(6,0) and ACNT(6,6). (e) Band gap as a function of $1/D$.

More interestingly, the spin moment of Cr atoms m_{Cr} is sensitive to the tube diameter D, as shown in Fig. 5(c). The increase in m_{Cr} from 2D counterpart to tube is evident and about 4% can be achieved in ZZNT(5,0) (with $D \sim 12.5$ Å). The narrower the tube, the larger the m_{Cr}, and $m_{Cr} \sim 1/D^2$ seems to fit well the calculation data. Such a curvature-enhanced spin moment is probably due to the distorted octahedral crystal field in the tubes. In consequence, Coulomb repulsion can surpass the crystal-field band gap Δ between the e_g and t_{2g} orbitals to increase the net spin moment. Such a hypothesis can be partly confirmed from the electronic band structure. As seen from Figs. 5(d) and 5(e), the band gap E_g decreases with decreas-

ing tube diameter D, suggesting that it becomes easier to cross the crystal field gap Δ to flip the spin when the tube becomes narrower. However, the relationship between E_g and the tube size D is quite opposite to that found in carbon nanotube,[26] which needs a further study.

4. Conclusion

In summary, we have studied the structural stability, electronic properties, and magnetic properties of low-dimensional nanoribbons and nanotubes of CrI_3 by *ab initio* density functional calculations. Ferromagnetic ordering is found to be stable in all the NR and NT structures of interest. An enhancement of the Curie temperature T_C can be expected when CrI_3 structure goes from 2D to NR/NT. The energy difference between the FM and AFM states can be improved by even up to 3 to 4 times in ZZNR, largely because of the electronic instability arising from a large DOS of I-5p orbitals at E_F. In NT structures, shrinking the tube size can reduce the crystal-field gap and drive a re-balance between spin majority and minority populations to harvest an enhancement of spin moment by up to 4%. Our theoretical results may give a guidance to the size and edge control of electronic and magnetic properties in low-dimensional magnetic devices.

References

[1] Novoselov K S, Jiang D, Schedin F, Booth T J, Khotkevich V V, Morozov S V and Geim A K 2005 *Proc. Natl. Acad. Sci. USA* **102** 10451

[2] Bora C, Bharali P, Baglari S, Dolui S and Konwar B 2013 *Comps. Sci. Technol.* **87** 1

[3] Novoselov K S, Geim A K, Morozov S V, Y. Jiang D, Zhang Y, Dubonos S V, Grigorieva I V and Firsov A A 2004 *Science* **306** 666

[4] Zhang Y B, Tan Y W, Stormer H L and Kim P 2005 *Nature* **438** 201

[5] Radisavljevic B, Radenovic A, Brivio J, Giacometti V and Kis A 2011 *Nat. Nanotechnol.* **6** 147

[6] Mak K F, Lee C, Hone J, Shan J and Heinz T F 2010 *Phys. Rev. Lett.* **105** 136805

[7] Splendiani A, Sun L, Zhang Y B, Li T S, Kim J, Chim C Y, Galli G and Wang F 2010 *Nano Lett.* **10** 1271

[8] Xiao D, Liu G B, Feng W, Xu X D and Yao W 2012 *Phys. Rev. Lett.* **108** 196802

[9] Espinosa A, Munoz-Noval A, Garcia-Hernandez M, Serrano A, de la Morena J, Figuerola A, Quarta A, Pellegrino T, Wilhelm C and Garcia M 2013 *J. Nanopart. Res.* **15** 1514

[10] Mermin N D and Wagner H 1966 *Phys. Rev. Lett.* **17** 1133

[11] Lee J U, Lee S, Ryoo J H, Kang S, Kim T Y, Kim P, Park C H, Park J G and Cheong H 2016 *Nano Lett.* **16** 7433

[12] Gong C, Li L, Li Z, Ji H, Stern A, Xia Y, Cao T, Bao W, Wang C, Wang Y, Qiu Z, Cava R J, Louie S G, Xia J and Zhang X 2017 *Nature* **546** 265

[13] Xing W Y, Chen Y Y, Odenthal P M, Zhang X, Yuan W, Su T, Song Q, Wang T Y, Zhong J N, Jia S, Xie X C, Li Y and Han W 2017 *2D Mater.* **4** 024009

[14] Wang Z, Zhang T Y, Ding M, Dong B J, Li Y X, Chen M L, Li X X, Huang J Q, Wang H W, Zhao X T, Li Y, Li D, Jia C K, Sun L D, Guo H H, Ye Y, Sun D M, Chen Y S, Yang T, Zhang J, Ono S, Han Z and Zhang Z D 2018 *Nat. Nanotechnol.* **13** 554

[15] Huang B, Clark G, Navarro-Moratalla E, Klein D R, Cheng R, Seyler K L, Zhong D, Schmidgall E, McGuire M A, Cobden D H, Yao W, Xiao D, Jarillo-Herrero P and Xu X D 2017 *Nature* **546** 270

[16] Klein D R, MacNeill D, Lado J L, Soriano D, Navarro-Moratalla E, Watanabe K, Taniguchi T, Manni S, Canfield P, Fernández-Rossier J and Jarillo-Herrero P 2018 *Science* **360** 1218

[17] Zhang Z D 2007 *Philosophical Magazine* **87** 5309

[18] Zhang Z D, Suzuki O and March N H 2019 *Advances in Applied Clifford Algebras* **29** 12

[19] Zhang Z D 2013 *Chin. Phys. B* **22** 030513

[20] Huang B, Clark G, Klein D R, MacNeill D, NavarroMoratalla E, Seyler K L, Wilson N, McGuire M A, Cobden D H, Xiao D, Yao W, Jarillo-Herrero P and Xu X D 2018 *Nat. Nanotechnol.* **13** 544

[21] Jiang S W, Li L Z, Wang Z F, Mak K F and Shan J 2018 *Nat. Nanotechnol.* **13** 549

[22] Seyler K L, Zhong D, Klein D R, Gao S Y, Zhang X O, Huang B, Navarro-Moratalla E, Yang L, Cobden D H, McGuire M A, Yao W, Xiao D, JarilloHerrero P and Xu X D 2018 *Nat. Phys.* **14** 277

[23] Dekker C 1999 *Phys. Today* **52** 22

[24] Lieber C M 1998 *Solid State Commun.* **107** 607

[25] Dresselhaus M S, Dresslhaus G and Avouris P 2001 *Carbon Nanotubes: Synthesis, Structure, Properties and Applications* (Berlin: Springer)

[26] Saito R, Dresslhaus G and Dresselhaus M S 1999 *Physical Properties of Carbon Nanotubes* (London: Imperial College Press)

[27] Son Y W, Cohen M L and Louie S G 2006 *Phys. Rev. Lett.* **97** 216803

[28] Son Y W, Cohen M L and Louie S G 2006 *Nature* **444** 347

[29] Ataca C, Sahin H, Akturk E and Ciraci S 2011 *J. Phys. Chem. C* **115** 3934

[30] Yang T, Okano S, Berber S and Tománek D 2006 *Phys. Rev. Lett.* **96** 125502

[31] Popov I, Yang T, Berber S, Seifert G and Tománek D 2007 *Phys. Rev. Lett.* **99** 085503

[32] Mihailovic D 2009 *Prog. Mater. Sci.* **54** 309

[33] Han X, Stewart H M, Shevlin S A, Catlow C R A and Guo Z X 2014 *Nano Lett.* **14** 4607

[34] Jiang W, Li S J, Liu H T, Lu G, Zheng F W and Zhang P 2019 *Phys. Lett. A* **383** 754

[35] Perdew J P, Burke K and Ernzerhof M 1996 *Phys. Rev. Lett.* **77** 3865

[36] Kresse G and Furthmüller J 2006 *Phys. Rev. B* **54** 11169

[37] Monkhorst H J and Pack J D 2006 *Phys. Rev. B* **13** 5188

[38] Liu J Y, Sun Q, Kawazoe Y and Jena P 2006 *Phys. Chem. Chem. Phys.* **18** 8777

[39] Hestenes M R and Stiefel E 1952 *J. Res. Natl. Bur. Stand.* **49** 409

[40] Jorio A, Dresselhaus M, Saito R and Dresselhaus G 2011 *Raman Spectroscopy in Graphene Related Systems* (New York: WileyVCH)

[41] Gr üneis A, Saito R, Samsonidze G G, Kimura T, Pimenta M A, Jorio A, Souza Filho A G, Dresselhaus G and Dresselhaus M S 2006 *Phys. Rev. B* **67** 165402

[42] Saito R, Nugraha A, Hasdeo E, Siregar S, Guo H H and Yang T 2015 *Phys. Status Solidi B* **252** 2363

[43] Stöhr J and Siegmann H C 2006 *Magnetism from Fundamentals to Nanoscale Dynamics* (Berlin: Springer)

[44] McGuire M A, Dixit H, Cooper V R and Sales B C 2015 *Chem. Mater.* **27** 612